Journal of Physics: Conference Series **2244** (2022) 012009 doi:10.1088/1742-6596/2244/1/012009

Measurement of ionization, charge exchange and ion confinement times in charge breeder ECR ion sources with short pulse 1+ injection of metal ions

M Luntinen[1], J Angot[2], O Tarvainen[3], V Toivanen[1], T Thuillier[2] and H Koivisto[1]

[1] University of Jyväskylä, Department of Physics, Survontie 9D, 40500 Jyväskylä, Finland
[2] Univ. Grenoble Alpes, CNRS, Grenoble INP, LPSC-IN2P3, 53 Avenue des Martyrs, 38000 Grenoble, France
[3] STFC ISIS Pulsed Spallation Neutron and Muon Facility, Rutherford Appleton Laboratory, Harwell, OX11 0QX, UK

E-mail: mailto:misapema@jyu.fi

Abstract. The Consecutive Transients (CT) method is used for estimating the characteristic times of ionization, charge exchange and confinement within the plasma of a Charge Breeder Electron Cyclotron Resonance Ion Source (CB-ECRIS). The method reveals differences in the characteristic times between different source configurations, with K^{9+} charge breeding efficiencies of 8.9 % and 20.4 %, and allows qualitative explanation of the improved breeding efficiency. The increase in K^{9+} efficiency is accompanied by a decrease in ionization time for low charge states, a decrease of charge exchange time for high charge states, and an overall decrease of the ion confinement time, which increases non-linearly with the charge state. The charge exchange time exhibits a minimum near charge state K^{8+}, indicating low neutral density near the plasma core. The CT-method yields a distribution of possible n_e and $\langle E_e \rangle$ corresponding to the spatial distribution of different charge state ions. The results hint at a non-uniform plasma electron density and energy distribution as well as a nested-layer distribution for the ion populations — hot and dense plasma with high charge state ions near the plasma core.

1. Introduction

The Consecutive Transients (CT) method has been used to obtain postdictions for the ionization, charge exchange and confinement times (τ^q_{inz}, τ^q_{cx} and τ^q) of charge state q ion populations in a CB-ECRIS plasma [1]. The method is based on measuring the extracted current transients prompted by short pulse injection of metal ions into the plasma, making fits to the transients of (minimum) five consecutive charge states, and an optimisation procedure to obtain the plasma electron density n_{e} and average energy $\langle E_{\mathrm{e}} \rangle$ of the presumed Electron Energy Distribution (EED) as well as the times τ^q_{inz}, τ^q_{cx} and τ^q. The method is based on the balance equation [2, 3] describing the temporal evolution of the densities of each ion population. The method probes the plasma conditions (n_e, $\langle E_{\mathrm{e}} \rangle$) of the support plasma, which determine τ^q_{inz}, τ^q_{cx} and τ^q of the injected ions. The results are spatially localised to the origin of the charge state q ion population. Measuring five consecutive charge state transients poses experimental limitations on the support/injected species combinations, since one must avoid q/m overlap in the Charge State Distribution (CSD). The method takes into account the uncertainty of the ionization cross section data and resulting

Table 1: The former (June 2020) and new (February 2021) charge breeder operating parameters.

	Configuration	
Parameter	Former	New
B_{inj} (T)	1.58	1.57
B_{min} (T)	0.45	0.44
B_{ext} (T)	0.83	0.84
μW power (W)	504	530
Support gas species	He	H_2
P_{inj} ($\times 10^{-8}$ mbar)	9.0	13.6
K^+ intensity (nA)	710	500
Injection pulse width (ms)	5	5

rate coefficients by the means of a Monte Carlo approach. No assumptions need to be made regarding the confinement scheme i.e. the functional dependence of τ^q.

Here we demonstrate that the CT-method can reveal the physical causes resulting in a change of the charge breeding efficiency. The comparison is made between the characteristic times obtained for potassium ions in the support plasma of a CB-ECRIS. The source configurations correspond to $^{39}K^{9+}$ efficiencies of 8.9 % and 20.4 %, respectively. Identifying the mechanisms underpinning the factor of > 2 improvement in the charge breeding efficiency of a stable isotope can guide the optimisation of Radioactive Ion Beam (RIB) production.

2. Experimental methods

The 1+→N+ test bench [4] at LPSC Grenoble is dedicated to the development and characterization of the Phoenix CB-ECRIS. The 1+ beam line is used for generating, characterizing and injecting the 1+ ion beam into the CB-ECRIS and the N+ beam line for analysing the extracted multicharged beams. The CB-ECRIS and the test bench are continuously upgraded to increase the global and charge state specific breeding efficiencies, Σ and η^q, and to reduce the charge breeding time and impurities in the N+ CSD. Short pulse injection of 1+ ions is used for the measurement of the charge breeding times τ_{CB}; the time when 90 % of all ions of charge state q have been extracted is designated as τ_{CB}[5]. In 2018-2019, the 1+→N+ test bench was upgraded to improve the vacuum and the alignment of the device [4]. The optimum efficiency of K^{10+} charge state measured in June 2020 was 10.6 % with τ_{CB}^{10+} of 132 ms. The first data using the CT-method to obtain the plasma parameters were taken in this configuration [1] with He support plasma.

The CB tuning and conditioning were then optimised to improve the CB efficiency to 20.4 % for K^{9+} with H_2 support gas (τ_{CB}^{9+} of 131 ms). The CT-method was applied in this configuration in February 2021 to estimate which parameters could have caused the efficiency improvement. Table 1 compares the two CB configurations. The main differences are the support gas species, the B_{min} value (+11.8%) and the microwave power (+5.2%). The charge breeding efficiencies η^q of the K charge states are shown in Table 2. A significant increase of K^{9+} efficiency was obtained (+11.5% absolute efficiency), accompanied by a small efficiency shift towards lower charge states. The extracted current transients of K^{3+}–K^{12+} were measured to obtain the characteristic times for K^{5+}–K^{10+} ion populations. The injected K^+ pulse was kept short (5 ms pulse width) and low in intensity (500 – 710 nA) to minimize the perturbance on the support plasma, while still resulting in high signal-to-noise ratio of the transient current.

Table 2: The charge breeding efficiencies η^q, charge breeding times τ^q_{CB} and the median values of the population confinement times τ^q. The global efficiency includes charge states K^{4+} – K^{12+}.

	η^q (%)		τ^q_{CB} (ms)		τ^q (ms)	
Ion	Former	New	Former	New	Former	New
K^{3+}	1.2	1.3	9	10		
K^{4+}	1.0	1.4	11	12		
K^{5+}	1.1	1.9	13	15	3	3
K^{6+}	1.2	3.0	16	49	3	4
K^{7+}	1.5	5.8	20	90	4	4
K^{8+}	2.7	11.1	45	119	15	12
K^{9+}	8.9	20.4	98	131	16	8
K^{10+}	10.6	11.8	132	138	24	12
K^{11+}	8.5	4.7	149			
K^{12+}	5.1	1.3	155			
Σ (%)	41.8	62.7				

3. Numerical methods

3.1. Principle of the method

The method for analyzing the measured beam current transients of the $q+$ ions has been extensively described in Ref. [1] and is only briefly recapitulated here: The balance equations [2, 3] governing the evolution in time of the ion population densities are defined by

$$\begin{aligned}\frac{\mathrm{d}n^q}{\mathrm{d}t} = &+n_e \left\langle \sigma v \right\rangle^{\mathrm{inz}}_{q-1\to q} n^{q-1} - n_e \left\langle \sigma v \right\rangle^{\mathrm{inz}}_{q\to q+1} n^q \\ &+n_0 \left\langle \sigma v \right\rangle^{\mathrm{cx}}_{q+1\to q} n^{q+1} - n_0 \left\langle \sigma v \right\rangle^{\mathrm{cx}}_{q\to q-1} n^q - \frac{n^q}{\tau^q},\end{aligned} \tag{1}$$

where the ionization and charge exchange rate coefficients ($\langle \sigma v \rangle^{\mathrm{inz/cx}}$) together with the plasma electron and neutral densities (n_e, n_0) determine the characteristic times

$$\tau^q_{\mathrm{inz}} \equiv \left[n_e \left\langle \sigma v \right\rangle^{\mathrm{inz}}_{q\to q+1} \right]^{-1} \tag{2}$$

$$\tau^q_{\mathrm{cx}} \equiv \left[n_0 \left\langle \sigma v \right\rangle^{\mathrm{cx}}_{q\to q-1} \right]^{-1} \tag{3}$$

and the loss term $-n^q/\tau^q$ defines the ion confinement time τ^q. Here n^q refer to the injected species, while n_e and n_0 are properties of the support plasma, which are assumed to be constant in time. Using the following identity [6, 7, 1] for the charge state q beam current

$$I^q = \kappa F_B L S \frac{n^q q e}{\tau^q}, \tag{4}$$

where κ is the beamline transmission efficiency, F_B a factor dependent on the mirror ratio of the ion source, L the length of the plasma chamber and S the area of the extraction aperture, one can recast the balance equation in the form

$$\frac{\mathrm{d}}{\mathrm{d}t} I^q = a_q I^{q-1} - b_q I^q + c_q I^{q+1}, \tag{5}$$

where I^{q-1}, and I^{q+1} are the beam currents of charge states $q-1$ and $q+1$, respectively, and the coefficients a_q, b_q and c_q are defined as

$$a_q = n_e \left\langle \sigma v \right\rangle^{\mathrm{inz}}_{q-1\to q} \frac{q}{q-1} \frac{\tau^{q-1}}{\tau^q} \tag{6}$$

$$b_q = \left(n_e \left\langle \sigma v \right\rangle^{\mathrm{inz}}_{q\to q+1} + n_0 \left\langle \sigma v \right\rangle^{\mathrm{cx}}_{q\to q-1} + 1/\tau^q \right) \qquad \text{and} \tag{7}$$

$$c_q = n_0 \left\langle \sigma v \right\rangle^{\mathrm{cx}}_{q+1\to q} \frac{q}{q+1} \frac{\tau^{q+1}}{\tau^q}. \tag{8}$$

The coefficients a_q, b_q and c_q can be determined by fitting Eq. 5 to the experimentally measured current I^q. The fitting is done by taking $I^{q-1}(t)$ and $I^{q+1}(t)$ as input parameters of Eq. 5, and solving the differential equation for the middle charge state current (numerical solution for the charge state q current denoted by $\mathfrak{I}^q(t)$). A least-squares method is then used to minimize the difference between $\mathfrak{I}^q$ and I^q to obtain a_q, b_q and c_q. Definitions 6, 7 and 8 then yield

$$\frac{q}{q+1} \frac{a_{q+1}}{n_e \left\langle \sigma v \right\rangle^{\mathrm{inz}}_{q\to q+1}} = \frac{b_{q+1} - n_e \left\langle \sigma v \right\rangle^{\mathrm{inz}}_{q+1\to q+2} - \frac{a_{q+1} c_q}{n_e \left\langle \sigma v \right\rangle^{\mathrm{inz}}_{q\to q+1}}}{b_q - n_e \left\langle \sigma v \right\rangle^{\mathrm{inz}}_{q\to q+1} - \frac{a_q c_{q-1}}{n_e \left\langle \sigma v \right\rangle^{\mathrm{inz}}_{q-1\to q}}}, \tag{9}$$

which is an equation of two unknowns, n_e and $\langle E_e \rangle$, since the rate coefficients $\left\langle \sigma v \right\rangle^{\mathrm{inz}}_{q'\to q''}$ may be calculated as a function of the average energy $\langle E_e \rangle$ of the EED. In lieu of experimental determination of the EED, we have thus far assumed the Maxwell-Boltzmann (MB) distribution. Equation 9 provides an infinitude of solutions for n_e and $\langle E_e \rangle$, which may be constrained on physical grounds such that

$$\begin{cases} \tau^q > 0, \\ \tau^{q+1} > 0, \\ 1/n_0 \left\langle \sigma v \right\rangle^{\mathrm{cx}}_{q\to q-1} > 0, \\ n_{e,\mathrm{low}} < n_e < n_{e,\mathrm{co}}, \\ \langle E_e \rangle_{\mathrm{low}} < \langle E_e \rangle < \langle E_e \rangle_{\mathrm{high}}\,, \end{cases} \tag{10}$$

where τ^q, τ^{q+1} and $\left[n_0 \left\langle \sigma v \right\rangle^{\mathrm{cx}}_{q\to q-1} \right]^{-1} \equiv \tau^q_{\mathrm{cx}}$ can be calculated from the definitions of a_q, b_q and c_q (c.f. Ref. [1] Eqs. (16) and (19)). The upper bound of n_e is the cut-off frequency [8] $n_{e,\mathrm{co}}$, while its lower bound $n_{e,\mathrm{low}}$ is taken from the literature [9]. The lower limit of $\langle E_e \rangle$ is set to be on the order of the plasma potential, i.e., ~ 10 eV, while its upper limit can be constrained at 10 keV, since the fraction of electrons found with energies above a few keV is 20–50 % [7, 10]. We thus focus on the warm electron population, which is mainly responsible for the ionization.

3.2. Code enhancements

While the numerical method has remained unchanged in principle since the introduction of the method [1], the code has been updated improving the precision and speed of the algorithm: *(i)* The rate coefficients are now calculated as a function of the average energy $\langle E_e \rangle$ of the EED (not T_e), which facilitates the comparison between different EEDs in the future. *(ii)* In Ref. [1] we adopted an "umbrella" uncertainty bound of 60 % for the rate coefficient as reported by Voronov [11]. The code now uses the experimental uncertainties of the cross section data [12]. *(iii)* The handling of the constraints has been improved: The penalty function is first minimized within the n_e and $\langle E_e \rangle$ bounds. After the minimum has been found, the characteristic times are calculated and minima leading to negative (unphysical) characteristic times are discarded. All the following results have been computed using the improved version (v1.2) of the code.

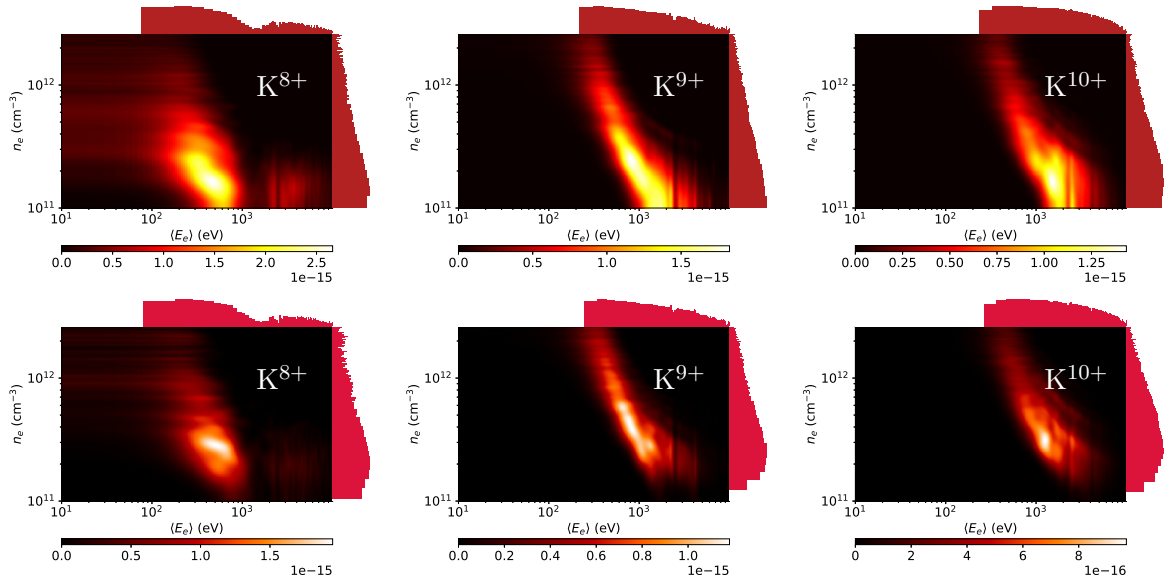

Figure 1: The $(n_e, \langle E_e \rangle)$ -solution sets of K8+–K10+ for the two charge breeder configurations Former (upper row) and New (lower row).

4. Results and analysis

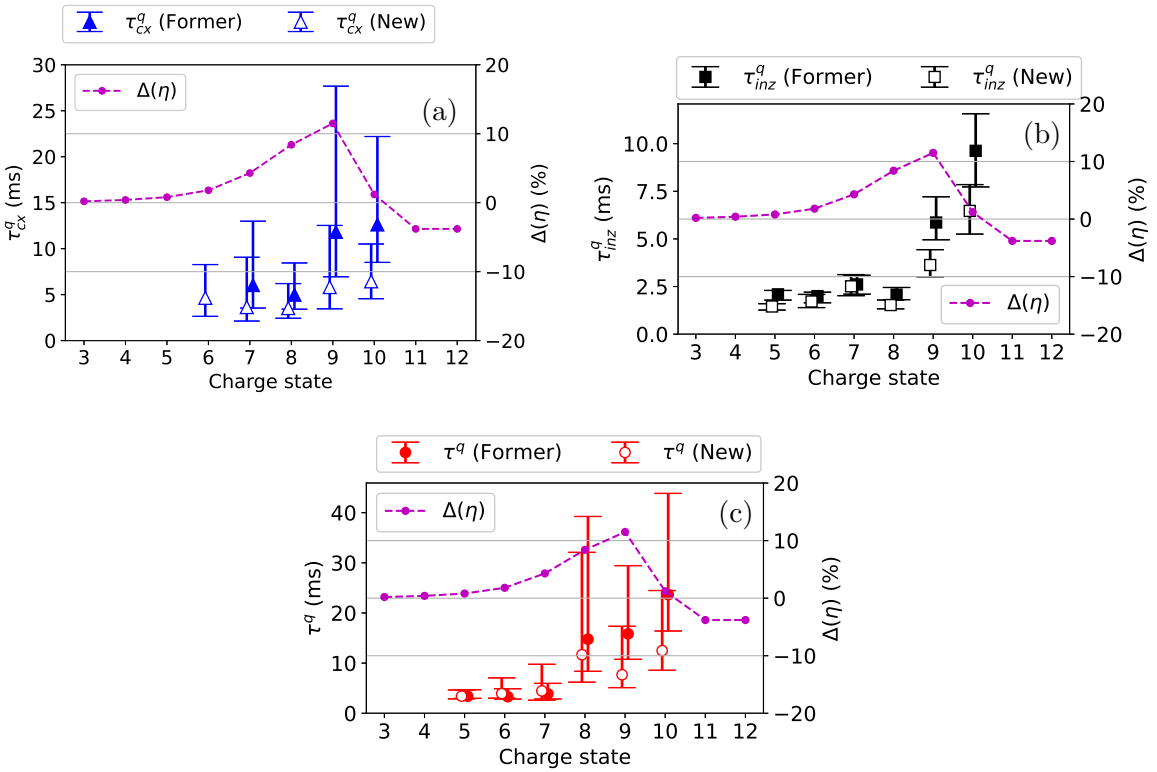

Figure 2: Comparisons of τ^q_{cx}, τ^q_{inz} and τ^q and the absolute difference $\Delta(\eta)$ of CB efficiencies.

Figure 1 shows heatmaps of the $(n_e, \langle E_e \rangle)$ i.e. viable solutions of Eq. 9 in both CB

Table 3: The most probable values of n_e and $\langle E_e \rangle$ in the two CB configurations.

	n_e ($\times 10^{11}$ cm^{-3})		$\langle E_e \rangle$ (eV)	
Ion	Former	New	Former	New
K^{5+}	1.0	1.0	96	129
K^{6+}	1.3	1.4	124	115
K^{7+}	1.2	1.0	156	168
K^{8+}	1.4	2.1	150	214
K^{9+}	1.0	2.6	288	357
K^{10+}	1.4	2.5	353	518

configurations for K^{8+}–K^{10+}. These examples represent the set of (n_e, $\langle E_e \rangle$)-pairs satisfying Eq. 9 in the vicinity of their respective ion population n^q. It must be recalled, that the I^q beams are extracted from the whole plasma, and the n_e and $\langle E_e \rangle$ values represent averages for a given ion population. The variation of the n_e and $\langle E_e \rangle$ as a function of q thus reflects the average spatial variation of each n^q. Hence, the characteristic times calculated at these (n_e, $\langle E_e \rangle$) also yield a distribution of results. Further constraining (if possible) of the n_e and $\langle E_e \rangle$ spans, and the uncertainty of the ionization cross sections, would decrease the uncertainty of the results. Histograms of the solution sets are projected onto the n_e and $\langle E_e \rangle$ axes (note the logarithmic scale).

Comparison of the histograms and the most probable values of n_e and $\langle E_e \rangle$ — tabulated in Table 3 — reveals that in the new configurations the local n_e and $\langle E_e \rangle$ are higher in particular for the HCIs. This is commensurate with the decrease of their τ^q_{inz}. Increase of n_e is also to be expected from the increased neutral gas input compared to the former configuration, as the increased n_0 allows for a higher n_e, particularly in the core of the plasma where the highly charged ions (HCIs) are believed to be confined in the potential dip [3], which itself is generated by the higher concentration of hot, well-confined electrons.

Figure 2 shows τ^q_{inz}, τ^q_{cx} and τ^q as a function of q for the two data sets. The characteristic times are overlaid with the absolute charge breeding efficiency change between the CB configurations. The uncertainty bounds enclose a one sigma (34.1 %) fraction of all results around the median value, represented by the data point. The distribution of values is typically sharply peaked around the lower values, with the most probable value lying below the median. The size of the uncertainty bounds is affected by both, the uncertainty of the experimentally measured ionization cross sections (e.g. at worst for K^{8+} the uncertainty is $\delta\sigma^{\text{inz}}_{q\to q+1}/\sigma^{\text{inz}}_{q\to q+1} = 200$ %) and the limits imposable upon the solution space ($n_e, \langle E_e \rangle$). Especially the K^{9+} efficiency is improved between the two configurations. Each of the characteristic times, in particular τ^q_{cx} and τ^q have decreased for the HCIs, although in most cases the uncertainty bounds overlap.

Molecular hydrogen has a larger diameter and smaller ionization potential than helium, which may explain the decrease in τ^q_{cx}, the charge exchange cross section being inversely proportional to the square of the ionization potential [13], i.e. $\sigma^{\text{cx}}_{q\to q-1} \propto I^{-2}$. Hence, switching to a H_2 support plasma increases $\sigma^{\text{cx}}_{q\to q-1}$. There is a minimum in τ^q_{cx} around K^{7+} and K^{8+} for both of the data sets. This minimum is attributable to the increase of $\sigma^{\text{cx}}_{q\to q-1}$ with q and the nested-layer structure of the ECRIS plasma. The latter is consistent with simulations and experiments [14, 15, 16, 17, 18] suggesting that the HCIs originate in the plasma core near the plasma chamber axis, while lower charge states originate from the peripheral plasma forming an overlapping layered structure. The increase of τ^q_{cx} towards the HCIs implies a decrease of neutral density toward the plasma core, since the $\sigma^{\text{cx}}_{q\to q-1}$ increasing with q would otherwise imply a further decrease in τ^q_{cx}. The decreased τ^q_{cx} of the HCIs is in line with the increased

charge breeding efficiency of the lower charge states in the new configuration.

There is a small decrease of τ^q_{inz} of the low charge states, while a prominent decrease, attributed to the increase of n_e implied by the solution sets (Fig. 1.), is seen for the HCIs in the new configuration. The effect of the faster ionization is to feed the high charge state populations. The electron shell closure at K^{9+} causes a discrete jump between τ^{8+}_{inz} and τ^{9+}_{inz}.

The median of the confinement time τ^q solutions has decreased in particular for K^{9+} and K^{10+}. Especially the former data set shows a non-linear q-dependence for τ^q. A linear model for τ^q would yield negative confinement times for low charge states, while a power law fit is found to best represent the results [1]. In Ref. [7] a linearly increasing trend and much shorter values (~ 5 ms) of τ^q were found. Short τ^q has been used as an argument in favor of a predominantly collisional or ambipolar ion confinement[19]. However, recent optical measurements of the Doppler broadening of ion emission lines [20] have found $\sim$ 10 eV ion temperatures, unattainable with such short τ^q. There is mounting evidence from emittance [15] and current density measurements [17, 18], simulations [14, 3], and afterglow experiments [21, 22], that the HCIs are confined within a potential dip $\Delta\phi$ of the plasma potential distribution. The HCIs remain confined until they obtain enough energy to overcome the electrostatic barrier, i.e. in excess of $eq\Delta\phi$. The electrostatic confinement scheme is in accordance with the power law trend observed here.

It is important to note that it is the combination of τ^q_{inz}, τ^q_{cx}, and τ^q ($\forall q \in \{0, 1, 2, \ldots, q_{\max}\}$) that determines the steady-state CSD of the plasma. The change in the K^{9+} efficiency can thus be explained through the characteristic times: *(i)* The decrease in τ^q_{cx} for the HCIs indicates faster rate of charge exchange and a consequent shift of the CSD towards lower charge states. In effect, the K^{9+} population is fed from the HCIs via charge exchange; *(ii)* The decrease in τ^q allows the K^{9+} ions — once produced — to escape more rapidly, which increases the extracted beam intensity; *(iii)* The shorter ionization time of the low charge states supplies to the K^{9+} population (but is counteracted by the simultaneous decrease of τ^q_{cx}). In short, the increase of the K^{9+} CB efficiency is explicable by the pile-up into $q = 9$ and its shorter confinement time.

5. Conclusion

It has been shown, that the CT-method can be used to discern differences between the characteristic times in different CB configurations. It therefore enables the analysis of fundamental processes in the ion source plasma. Here, the source tune has been changed by varying multiple operating parameters, and the characteristic times are affected by multiple physical effects. In future experiments, the evolution of the characteristic times will be studied by varying one parameter at a time.

It must be noted that an infinitude of $(n_e, \langle E_e \rangle)$ pairs satisfies Eq. 9. It would be a great benefit to the method, if it were possible to set stricter constraints on n_e and $\langle E_e \rangle$, and if the ionization cross section were known more precisely. The presumed EED also being a source of possible error, its experimental measurement in plasma is desired. In short term we plan to study the sensitivity of the results on the assumed EED.

The CT-method provides a breakdown of τ^q_{CB} to its components: The characteristic times τ^q_{inz}, τ^q_{cx} determine the rate at which ions of different charge states are generated, while τ^q gives the rate at which ions of a given population exit the plasma. It is important to note that τ^q_{CB} is affected by the characteristic times of all charge states populations as a given particle may spend time as an ion at various different charge states before being extracted from the source. The τ^q_{CB} is thus a measure of the cumulative confinement time [23] of an ion, including its charge state history, while τ^q measures the confinement time of ion population at charge state q, and is directly affected by changes in the ion confinement conditions.

Based on the discussion of the causes underlying the change in K^{9+} efficiency, it can be said that in order to maximize the charge breeding efficiency of a given charge state one must maximize the pile-up into that charge state population the charge states both above and below,

i.e. one must minimize the ionization time from below, and minimize the charge exchange time from above. The best efficiencies can be obtained for charge states whose valence electron lies on a closed shell (such as K^{9+}), because the ionization from such a state is minimized and the population will not be depleted as much via ionization to higher states. At the same time one should minimize the confinement time of the desired charge state to efficiently extract the ions.

Data availability statement

The data that support the findings of this study are openly available at `DOI:10.6084/m9.figshare.14685432`, and the analysis code (release version 1.2.4) is publicly available at: `https://github.com/misapema-jyfl/popTauPy`.

Acknowledgments

We acknowledge grants of computer capacity from the Finnish Grid and Cloud Infrastructure (persistent identifier urn:nbn:fi:research-infras-2016072533).

References

[1] Angot J, Luntinen M, Kalvas T, Koivisto H, Kronholm R, Maunoury L, Tarvainen O, Thuillier T and Toivanen V 2020 *Plasma Sources Science and Technology* **30** 035018
[2] Shirkov G, Mühle C, Musiol G and Zschornack G 1991 *Nucl. Instrum. Methods Phys. Res. A: Accel. Spectrom. Detect. Assoc. Equip.* **302** 1 – 5 ISSN 0168-9002
[3] Shirkov G D 1993 *Plasma Sources Science and Technology* **2** 250–257
[4] Angot J, Galatà A, Maunoury L, Thuillier T, Baylac M, Migliore M and Sole P 2020 *ECRIS 2020 proceedings WEZZO02*
[5] Angot J, Tarvainen O, Thuillier T, Baylac M, Lamy T, Sole P and Jacob J 2018 *Phys. Rev. Accel. Beams* **21**(10) 104801
[6] West H J 1982 Calculation of ion charge state distribution in ecr ion source Tech. rep. Lawrence Livermore National Laboratory
[7] Douysset 1 G, Khodja H, Girard A and Briand J P 2000 *Phys. Rev. E* **61**(3) 3015–3022
[8] Geller R 1996 *Electron cyclotron resonance ion sources and ECR plasmas* (IOP) ISBN 9780750301077
[9] Tarvainen O, Koivisto H, Galatà A, Angot J, Lamy T, Thuillier T, Delahaye P, Maunoury L, Mascali D and Neri L 2016 *Phys. Rev. Accel. Beams* **19**(5) 053402
[10] Perret C 1998 *Caractérisation de la population électronique dans un plasma de source d'ions à résonance cyclotronique électronique* Ph.D. thesis Université Joseph Fourier, Grenoble
[11] Voronov G 1997 *At. Data Nucl. Data Tables* **65** 1 – 35 ISSN 0092-640X
[12] Lennon M A, Bell K L, Gilbody H B, Hughes J G, Kingston A E, Murray M J and Smith F J 1988 *Journal of Physical and Chemical Reference Data* **17** 1285–1363 ISSN 15297845
[13] Knudsen H, Haugen H K and Hvelplund P 1981 *Phys. Rev. A* **23**(2) 597–610
[14] Mironov V, Sergey B, Bondarchenko A, Efremov A and Loginov V 2015 *Physical Review Special Topics - Accelerators and Beams* **18**
[15] Wutte, D, Clark, D J, Laune, B, Leitner, M A, Lyneis C M 2001 *AIP Conference Proceedings* vol 445 pp 445–448
[16] Leitner M A, Wutte D and Lyneis C M 2001 *Proceedings of the 2001 Particle Accelerator Conference, Chicago* vol 5 ed Lucas P and Webber S Argonne National Laboratory and Fermi National Accelerator and Laboratory Oak Ridge National Laboratory (Chicago, Illinois U.S.A.: IEEE) pp 67–69
[17] Panitzsch L, Stalder M and Wimmer-Schweingruber R F 2011 *Rev. Sci. Instrum.* **82** 033302
[18] Panitzsch L, Peleikis T, Stalder M and Wimmer-Schweingruber R F 2011 *Rev. Sci. Instrum.* **82** 093302
[19] Melin G, Drentje A G, Girard A and Hitz D 1999 *Journal of Applied Physics* **86** 4772
[20] Kronholm R, Kalvas T, Koivisto H, Laulainen J, Marttinen M, Sakildien M and Tarvainen O 2019 *Plasma Sources Science and Technology* **28** 075006
[21] Sortais P 1992 *Rev. Sci. Instrum.* **63** 2801–2805
[22] Nakagawa T *et al.* 1998 *Review of Scientific Instruments* **69** 637–639
[23] Marttinen M *et al.* 2020 *Rev. Sci. Instrum.* **91** 013304